

Morphological and Structural Investigation of Sexithiophene Growth on KCl (100)

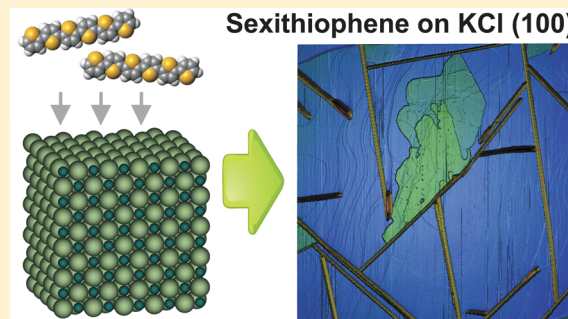
Günther Schwabegger,^{*,†} Tatjana Djuric,[‡] Helmut Sitter,[†] Roland Resel,[‡] and Clemens Simbrunner[†]

[†]Institute of Semiconductor and Solid State Physics, Johannes Kepler University, Altenbergerstrasse 69, A-4040 Linz, Austria

[‡]Institute of Solid State Physics, Graz University of Technology, Petersgasse 16, A-8010 Graz, Austria

Supporting Information

ABSTRACT: The morphology and structure of sexithiophene deposited on KCl (100) substrates was investigated by scanning force microscopy and specular X-ray diffraction measurements. Two different needle-like structures with {010} and {411} contact planes have been observed as well as islands of almost upright standing sexithiophene molecules with a {100} contact plane. Furthermore an azimuthal alignment of all three crystal orientations was observed by X-ray diffraction pole figure measurements, and the growth directions reflect the 4-fold rotational symmetry of the substrate surface. In addition the analysis of crystals with {411} and {100} contact planes unveiled that they share a common crystallographic direction which is explained by ledge directed epitaxy.



INTRODUCTION

In recent years a lot of effort has been undertaken in order to prepare and investigate ordered structures of π -conjugated organic molecules on nanoscopic and mesoscopic scales. The interest of both fundamental and applied science was mainly driven by the goal to understand and improve the properties of materials used for organic electronics (e.g., light emitting diodes,^{1–3} field effect transistors^{4–6} and solar cells^{7,8}) and to establish novel systems for optical applications (e.g., wave-guiding and lasing^{9–13}). Frequently small rodlike molecules like oligothiophenes, oligoacenes and oligophenylenes have been selected as model systems. In the group of oligothiophenes sexithiophene (6T) has shown interesting high quality properties like a charge carrier mobility of up to $0.1 \text{ cm}^2/(\text{V s})$.^{14,15} Consequently there has been an interest in understanding the growth mechanism of such molecules on well-defined model substrates like single crystalline Cu,¹⁶ sheet silicates¹⁷ or patterned SiO₂.¹⁸

The study in this paper aims at providing a conclusive picture of the formation of 6T nanostructures by an in-depth analysis of the growth on an alkali-halide single crystal, namely potassium chloride (KCl).

EXPERIMENTAL PROCEDURES

KCl Substrate. Freshly cleaved KCl has been used as a substrate for our epitaxial studies. KCl exhibits a face centered cubic crystal structure with a lattice constant of 6.36 \AA .¹⁹ The unit cell of the (100) surface can be described by the 2D-space group $p4mm$ as shown in Figure 1. Importantly, this high symmetry surface exhibits rotation centers of order 2 and 4 as well as mirror and gliding planes. It is expected that the symmetry of the substrate will be reflected in the multiplicity of epitaxial alignments of the deposited molecules.²⁰

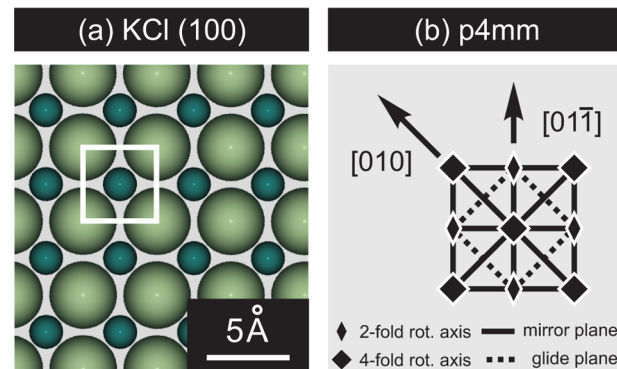


Figure 1. (a) The (100) surface of the KCl crystal, with the white rectangle illustrating the surface unit cell. Smaller spheres representing Cl atoms and bigger spheres representing K atoms. (b) The $p4mm$ symmetry of the surface unit cell including the respective symmetry elements.

Sample Preparation. The hot wall epitaxy (HWE) technique was applied for the deposition of the organic material, which allows the growth process to be performed close to thermodynamic equilibrium, and in further consequence relatively high vapor pressure of the organic deposit in the substrate region can be achieved. Therefore the requirements concerning vacuum conditions are reduced as compared to, e.g., molecular beam epitaxy.²¹ The source material 6T was purified twice by thermal sublimation before filling it into the quartz tube of the HWE reactor. KCl substrates were transferred into the deposition chamber via a load lock and subsequently preheated at the deposition

Received: July 30, 2012

Revised: November 14, 2012

Published: December 24, 2012

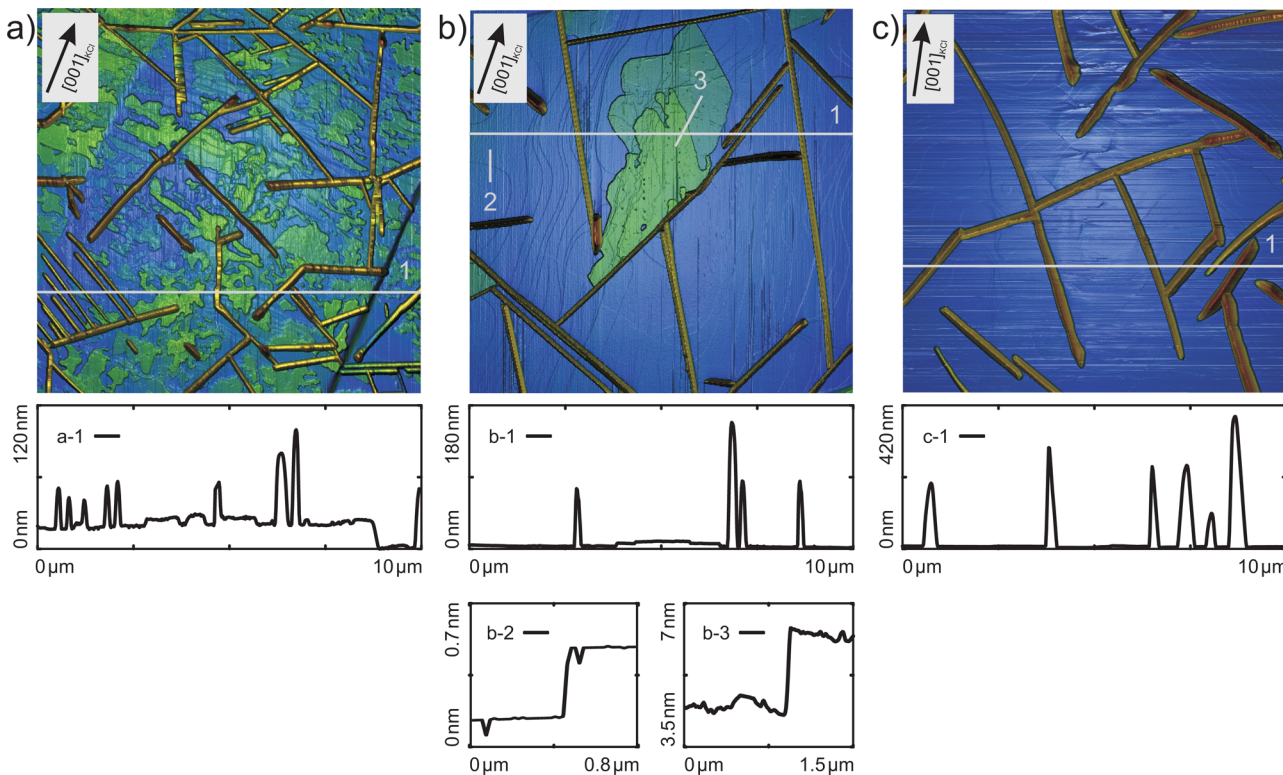


Figure 2. $10 \times 10 \mu\text{m}^2$ scanning force microscopy analysis of sexithiophene on KCl showing rendered images in highly nonlinear color coding and profiles indicating the relevant height levels. KCl crystallographic directions have been deduced by comparing Fourier transformations of the images with the results from XRD analysis revealing the orientation of needles with respect to KCl high symmetry directions. The directions are estimated with an accuracy of $\pm 5^\circ$. Thin film deposition was performed at the following substrate temperatures: (a) 60°C , (b) 90°C and (c) 135°C .

temperature ($60\text{--}135^\circ\text{C}$) for 30 min to clean the surface from adsorbed species and to ensure a stable temperature during the whole deposition process. The deposition was performed thereafter under a base pressure of 9×10^{-6} mbar at a nominal deposition rate of 0.4 nm/min.

X-ray Diffraction. X-ray diffraction (XRD) measurements were carried out on a Philips X'pert X-ray diffractometer using Cr $\text{K}\alpha$ radiation ($\lambda = 2.29 \text{ \AA}$) and a secondary graphite monochromator. Specular scans were performed in Bragg–Brentano configuration by varying the z -component of the scattering vector q . Consequently it is possible to detect lattice planes which are parallel to the sample surface. X-ray diffraction pole figure measurements were performed in Schultz reflective geometry.²² Pole figures are acquired by measuring at a constant length of q and only varying its direction. The Schmidt projection is used to map the poles.

Based on both the observed Bragg peaks of the specular scan and the direction of the poles (net-plane normals) within the pole figures, the involved crystallographic phases as well as the azimuthal alignment of the crystallites with respect to the substrate can be identified.

Simulations of XRD pole figures were performed by a custom-made software.

Morphological Investigation. Optical microscope images have been acquired by a Nikon Labophot 2A microscope in combination with a Nikon Type 115 digital camera.

Scanning force microscopy (SFM) studies of the deposited organic films were performed using a Digital Instruments Dimension 3100 in the tapping mode. The images have been acquired at scan speeds of $4\text{--}6 \mu\text{m/s}$ using SiC tips exhibiting a cone angle of 40° . Nominal values for resonance frequency and tip radius are 325 kHz and 10 nm respectively.

EXPERIMENTAL RESULTS

Morphological Investigation. Morphological investigations have been performed on a set of samples prepared by

depositing 6T for 30 min at various substrate temperatures ranging from 60 to 135°C . On each sample an SFM image of the size of $10 \times 10 \mu\text{m}^2$ has been collected and analyzed.

Figure 2 depicts three representative images, taken on films deposited at a substrate temperature of (a) 60°C , (b) 90°C and (c) 135°C . The images reveal different structures, namely, flat islands (visualized in green color) and needle-like structures (yellow and red). Qualitatively it is visible that the cross-sectional area of the needles is increasing with increasing substrate temperature. For instance, the height of the needles is strongly increasing from $\approx 50 \text{ nm}$ to maximum values of $\approx 400 \text{ nm}$. This finding is accompanied by a reduction in the number of the needles and additionally the number of islands is reducing with increasing substrate temperature as well. Furthermore, cleavage steps of different sizes are found on the surface. The biggest ones are in the order of 20 nm as visible in the bottom right corner of Figure 2a. The smallest size of cleavage steps is shown in profile b-2 of Figure 2 exhibiting a size of $\approx 4 \text{ \AA}$, which fits well to a monolayer of the KCl substrate.

Taking a closer look at the cross section of the island depicted in profile b-3 of Figure 2, we can clearly distinguish between different height levels and we observe a step height of 2.2 nm. The height of the layer can be explained, because it is close to the length of upright standing 6T molecules with their (100) facet parallel to the surface. A comparable observation has been reported for 6T deposited on muscovite mica.^{23,24} Consequently it is reasonable to assume that these islands are composed of upright standing molecules.

In the case of the needles, differences in height and cross-sectional shape of the needles have been observed. For instance

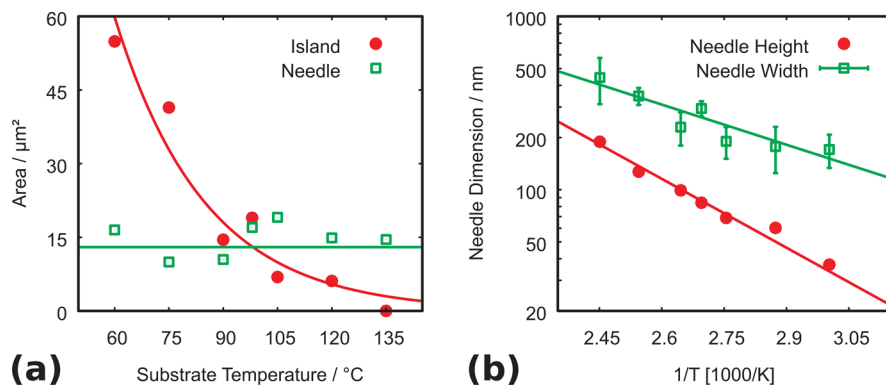


Figure 3. (a) Projected area of needles (green rectangles) and islands (red circles) versus substrate temperature. The solid lines act as a guide to the eye. (b) Arrhenius plots of needle width (green rectangles) and needle height (red circles) with respect to inverse substrate temperature. Solid lines represent linear fits.

it was found that some needles have an asymmetric shape with one facet that is more steep than the other, as visible in the profile of Figure 2c. A similar finding was already reported in a previous work of our group, where 6T has been deposited on muscovite mica.¹⁷ Therein it was unveiled by cross-sectional transmission electron microscopy, that structures appearing needle-like in SFM are in reality consisting of tilted lamellae. This discrepancy is caused by the fact that an SFM image is not only consisting of topographical features of the surface but it is rather obtained by a convolution of the shape of the tip and the surface. Consequently one observes a shadow effect in the case of a tilted entity.

These slight differences do not allow assignment of the morphologies to distinct crystallographic structures such as 6T crystals with a $\{\bar{4}11\}$ or a $\{010\}$ contact plane, which have been reported for instance on Cu (010).¹⁶ Therefore this issue will be clarified later on by XRD measurements.

Based on the previous findings we conducted a quantitative analysis of the SFM images. The projected surface area of both islands and needles with respect to the chosen surface temperature of the substrate has been determined. As depicted in Figure 3a we found that the reduction in the number of needles is compensated by the growth in width, giving an approximately constant value for the needle area of $14.6 \pm 3.3 \mu\text{m}^2$. On the other hand a completely different behavior for the evolution of island area with varying substrate temperature was observed. In this case the area covered by the respective structures is declining with increasing substrate temperature. At 135°C we cannot find any island on the $10 \times 10 \mu\text{m}^2$ SFM scan. On a much larger image taken with an optical microscope we observe a few islands (see the Supporting Information). Nevertheless these structures are expected to vanish completely at even higher substrate temperatures.

We further determined average values for needle width and height for this sample series. In the case of needle width, the evaluation was performed by collecting the values from cross-sectional profiles of a large set of needles and subsequently calculating average values. In the case of needle height, the total needle volume was computed and divided by their surface area, which gives an average needle height. Plotting both height and width of these structures in an Arrhenius type of diagram reveals an activated process for their formation as shown in Figure 3b. The activation energy for needle growth in height and width was found to be $0.26 \pm 0.02 \text{ eV}$ and $0.15 \pm 0.04 \text{ eV}$ respectively. Values in this range are expected as comparable

numbers have been reported for the growth of *p*-hexaphenyl on muscovite mica (001).²⁵

It has to be stated that we determined activation energies ignoring the existence of different types of needles (different crystal contact planes are observed by XRD investigations presented in the next section). Nevertheless Figure 3b shows a clear Arrhenius behavior and not a superposition of curves with unequal slopes for different temperature regimes. One possible explanation for this observation would be a clear domination in quantity of one type of needle, but this can be excluded due to similar peak intensities found by X-ray analysis for both needle types. Therefore we conclude that similar activation energies for both types of needles are causing the observed thermally activated behavior.

Structural Investigation. SFM analysis already indicated different crystal orientations present on the KCl (100) surface. In order to identify them, XRD investigations have been performed on samples prepared at substrate temperatures of 90 and 135°C . Further a clean substrate was analyzed as a reference. As a first step specular scans have been carried out, which allows one to find crystallographic planes that are parallel to the substrate surface. The peak positions in the specular scans as shown in Figure 4 can be explained by a 6T low temperature phase. This phase exhibits a monoclinic unit cell (space group $P2_1/n$) with the following parameters: $a = 44.708 \text{ \AA}$, $b = 7.851 \text{ \AA}$, $c = 6.029 \text{ \AA}$ and $\beta = 90.76^\circ$.²⁶

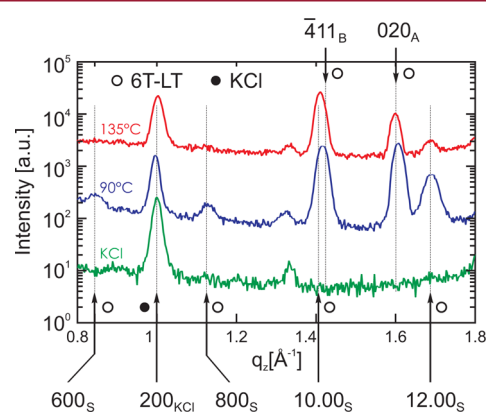


Figure 4. Specular scan of a sexithiophene thin film prepared at a substrate temperature of 90°C (blue line) or 135°C (red line) and of a bare KCl substrate (green line). Peaks are indicated by arrows accordingly. For clarity the measurements are shifted vertically.

The peak located at $q_z = 0.99 \text{ \AA}^{-1}$ is originating from the KCl substrate, and the peak at $q_z = 1.60 \text{ \AA}^{-1}$ can be assigned to crystallites whose relationship to the KCl substrate can be described by a $\{010\}$ contact plane. According to the nomenclature used by Koini et al. this crystal orientation will be labeled type A.¹⁶ Furthermore, we observe peaks originating from 6T crystals oriented with their $\{100\}$ net planes parallel to the substrate surface (type S). The respective series of $2n.00$ peaks are indicated in Figure 4. After analyzing the peak intensities of the $2n.00$ series, we found that the peak at $q_z = 1.41 \text{ \AA}^{-1}$ is stronger than expected. Therefore we conclude that another crystallographic component is partly responsible for the high intensity of this peak. The reflection pattern of 6T crystals oriented with their $\{\bar{4}11\}$ net planes parallel to the substrate surface would explain this finding (type B). The presence of crystal type B will be confirmed later on by XRD pole figure measurements.

Crystallites of those three types have been reported before on various substrates: Crystals of type S consist of almost upright standing molecules forming flat island-like structures (e.g., on Cu (110),¹⁶ muscovite mica²⁷ or SiO₂²⁸). Comparing the size of the (12.00) peak we can also observe that this structure is less present at higher substrate temperature, which verifies the results found by SFM. Type A is characterized by molecules with their long molecular axis (LMAs) parallel to the surface and has been reported to form needle-like structures on Cu (110)¹⁶ and TiO₂ (110).²⁹ Crystallites of type B have been observed on Cu (110)¹⁶ and muscovite mica (001).¹⁷ Similar to type A they form anisotropic needle shaped structures consisting of almost flat lying molecules.

Azimuthal Alignment of Crystallites. To determine the preferential azimuthal alignment of the crystallites with respect to the substrate, we have performed pole figure investigations. Additionally these measurements allow one to definitely prove the existence of crystal type B on the samples. In Figure 5a–c the measurements for the $\{\bar{4}11\}$, $\{\bar{3}11\}$ and $\{\bar{2}11\}$ pole figures are shown in the left panels. Since there are only spotlike reflections visible and no diffraction rings, it follows that all crystal structures which are formed by the deposited 6T molecules are in a discrete azimuthal alignment with respect to the substrate. An in-depth analysis of the reflection spots is depicted in the right panels of Figure 5a–c. A simulation of the position of the diffraction peaks is shown, assuming crystallites of types A, B and S on a KCl (100) surface. The simulations are in good agreement with the measurements, especially the spots that correspond to needle-like crystallites of types A (indexed by hexagons) and B (indexed by circles) can be clearly resolved. Please note that reflections originating from crystals exhibiting different contact planes are expected to appear in the same pole figure, if the scanned net planes have equal lattice spacing. As indexed by black solid circles in Figure 5, we were also able to detect the reflection peaks of the KCl $\{101\}$ net planes. Consequently it is possible to determine the orientation of the crystals with respect to KCl.

Reflection spots originating from crystals of type S (indexed by rectangles) are only faintly visible in the measurements presented in Figure 5. To confirm them more reliably pole figure measurements for the $\{120\}$ and $\{011\}$ net planes were performed (see Supporting Information). This data additionally substantiates the existence of crystal type S on the investigated sample.

To summarize the results obtained from pole figure measurements, we can conclude that the detected organic

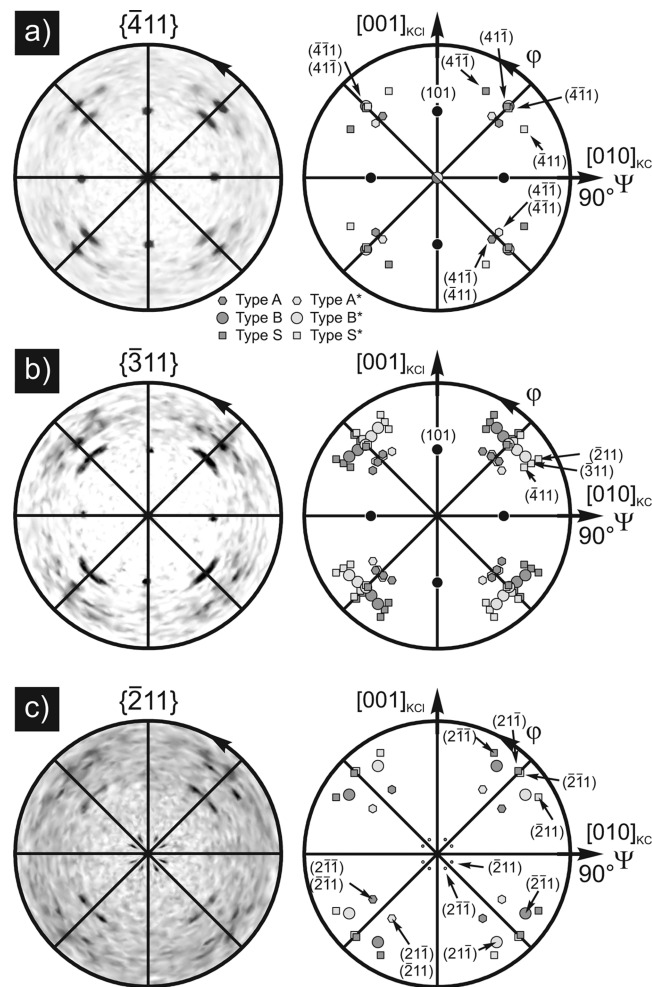


Figure 5. Measured (left) and simulated (right) XRD pole figures of the (a) $\{\bar{4}11\}$, (b) $\{\bar{3}11\}$ and (c) $\{\bar{2}11\}$ net plane normals (poles). Reflections of crystal type A are indexed with hexagons, type B with open circles and type S with rectangles. Symmetry equivalent crystals denoted by A*, B* and S* exhibiting contact planes of $\{0\bar{1}0\}$, $\{\bar{4}11\}$ and $\{\bar{1}00\}$, respectively, are formed due to mirror axis of the substrate surface (black lines). Peaks originating from the KCl substrate are shown as full circles. The measurements are performed on a 6T layer prepared at a substrate temperature of 90 °C.

nanostructures follow the 4-fold rotational symmetry of the KCl (100) substrate surface. Furthermore the proposed crystal structures of types A/B/S with their $\{\bar{4}11\}/\{010\}/\{100\}$ contact planes have been assured.

Real Space Model. Using the results from XRD measurements together with the knowledge of the orientation of the molecules relative to the crystallographic unit cell from single crystal solutions,²⁶ the real space orientation of the molecules relative to the KCl (100) surface is derived and presented in the following.

Crystals of type A are characterized by a long needle axis (LNA) along the $[001]$ direction of the 6T crystal. This direction is determined by the intersection of the contact plane and the low energy surface which is always a facet along the LNA. In case of 6T it is known that the low energy surface is given by a (100) net plane.²⁶ One can find two symmetry equivalent crystals with (010) and ($\bar{0}10$) contact planes, which is depicted in Figure 6a. Their LNAs are rotated by $\pm 20.6^\circ$ with respect to the KCl high symmetry directions ($[001]_{\text{KCl}}$ and

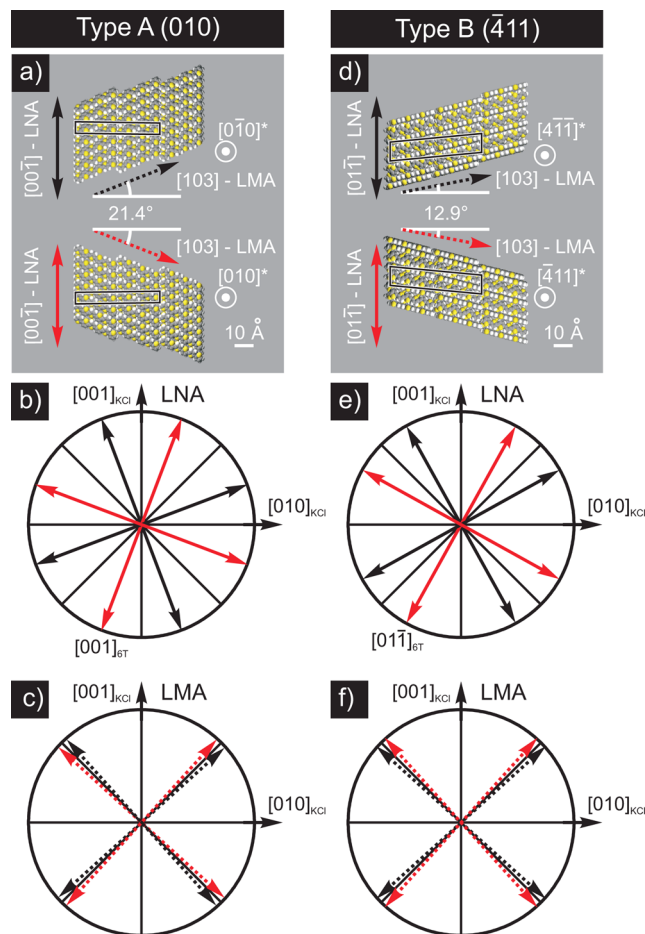


Figure 6. (a) Top view of the real space model of the type A crystal. Due to the mirror symmetry two equivalent crystals are found on the substrate. Long needle axis (LNAs) and long molecular axis (LMAs) associated with $\{010\}$ contact planes are shown in red and for the $\{010\}$ contact planes in black respectively. (b) Experimentally observed directions for the LNAs. Black solid lines represent mirror axis of the KCl (100) surface. (c) Determined directions for the LMAs. (d–f) A similar real space model for crystals of type B.

$[0\bar{1}0]_{\text{KCl}}$) as depicted in Figure 6b. Since the angle between the LNA and the LMA ($[00\bar{1}]_{\text{6T}}$) in a type A crystal is 68.6° , it is possible to calculate the orientation of the LMAs. The LMAs are rotated by $\pm 42^\circ$ with respect to $[001]_{\text{KCl}}$ and $[010]_{\text{KCl}}$ as shown in Figure 6c. Consequently the LMAs of the 6T molecules are almost parallel to $[011]_{\text{KCl}}$ and $[01\bar{1}]_{\text{KCl}}$ which is very similar to the alignment found for *p*-hexaphenyl on KCl (100). *p*-Hexaphenyl molecules are oriented perfectly parallel to these high symmetry directions of the KCl substrate as reported by Haber et al.³⁰

As depicted in Figure 6d–f crystals of type B are characterized by a LNA along the $[01\bar{1}]$ direction of the 6T crystal, which are rotated by a value of $\pm 29.1^\circ$ with respect to $[001]_{\text{KCl}}$ and $[010]_{\text{KCl}}$. Interestingly, the LMAs are exactly in the same position as in the case of crystals of type A (compare Figures 6c and 6f), which represents a hint that this alignment is the initial adsorption direction of 6T on KCl.

Azimuthal alignment for island-like crystals of type S was also observed, and interestingly they share their $[0\bar{1}1]$ direction with needles of type B, which is presented in detail in Figure 7. In a side view it is visible that not only do the crystals share a common orientation on the substrate but the tilt angle of

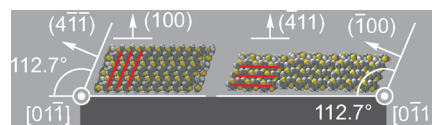


Figure 7. Real space models of sexithiophene crystals with (100) (standing molecules) and ($\bar{4}11$) (lying molecules) contact planes. The substrate is sketched in dark gray, and the needle growth direction is perpendicular to the plotting plane. The crystals consisting of standing and lying molecules exhibit the same tilt angles of their facets, and they share a common growth direction ($[01\bar{1}]$ and $[0\bar{1}1]$). Red lines indicate long molecular axis.

112.7° of the LMAs in the island-like crystals of type S is perfectly fitting to the inclination of the (001) plane of the needles of type B. Most likely the islands nucleate on the sidewalls of already existing needles. Such epitaxial alignment based on a geometrical fit between nucleating crystallites and already existing topographic features on the substrate is called “ledge directed epitaxy”.^{31,32}

Optical Micrographs. Further investigations of the azimuthal alignment of the needle-like crystallites are presented in the following. Optical microscopy has been chosen for this purpose because it provides a better statistical resolution as compared to $10 \times 10 \mu\text{m}^2$ SFM images. In Figure 8a the image

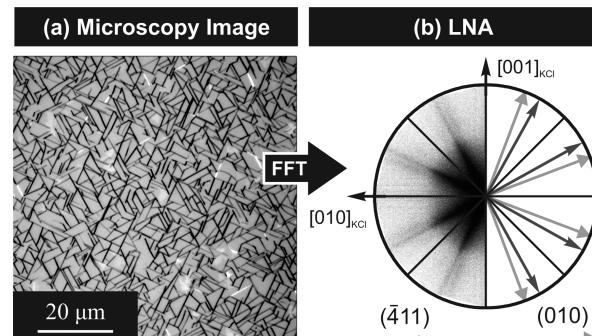


Figure 8. (a) Optical microscope image of sexithiophene deposited on KCl (100) (105°C substrate temperature). (b) Fourier transformation revealing the long needle axis (LNAs) present in the image. The different orientations of LNAs for needles of type A (010) and type B ($\bar{4}11$) are sketched as deduced from X-ray diffraction pole figure analysis.

of the sample prepared at a substrate temperature of 105°C is depicted. We can clearly observe well ordered needle-like structures appearing mostly in dark and additionally more diffuse bright areas that are interpreted as flat islands as also observed in SFM images. Motivated by the existence of preferential needle orientations we performed an FFT analysis of these images (depicted in Figure 8b).

As expected, the 4-fold symmetry of the KCl substrate is clearly reflected in the FFT pattern. We found two peaks in intensity located relatively close to each other, which we assign to the LNAs of crystal types A and B (compare Figures 6b and 6e). Similar pictures have been obtained on all prepared samples irrespective of the used substrate temperatures (see the Supporting Information). Since we do not see any qualitative change in the needle-like structures if the substrate temperature is varied, it seems justified to generalize the conclusions which have been drawn from XRD analysis of the 90 and 135°C samples to the entire investigated temperature range.

Comparison between 6P and 6T Thin Film Growth on KCl (100). As 6P and 6T molecules are structurally relatively similar, it seems interesting to compare the behavior of these molecules if they are deposited on KCl (100).

In this work, we observed both standing and flat lying 6T molecules. In the latter case we found two different crystal contact planes, namely, (010) and (411). Similarly for 6P there are reports of standing molecules forming flat islands exhibiting a (001) contact plane, and there are three crystal types with almost flat lying molecules forming needle-like structures, namely, (111), (112) and (203).^{33–35}

If we compare the alignment of 6P and 6T molecules in the case of lying molecules, large similarities are observed. For 6T the LMA is oriented almost exactly along the [011]_{KCl} directions, only showing $\pm 3^\circ$ azimuthal split with respect to the mentioned KCl high symmetry direction. Interestingly in the case of 6P it was reported that the molecules do align perfectly along [011]_{KCl}.^{30,35}

The only clear difference in the behavior of the two molecules on KCl (100) can be seen if we take a look at the evolution of the relative abundance of different crystal contact planes with respect to substrate temperature. In the case of 6T we do observe a decreasing surface coverage of islands (standing molecules) with increasing substrate temperature, which is accompanied by the increase in cross-sectional dimensions of needle-like structures (lying molecules). Such behavior is not reported for 6P, but in fact it is the opposite. Increased substrate temperature during growth tends to promote the formation of islands at the expense of needles covering the surface. Such behavior was observed both by SFM studies^{34,36} and by XRD analysis.^{33,35}

■ CONCLUSION AND DISCUSSION

In this paper we reported on epitaxial growth of 6T on KCl (100), which was examined by crystallographic and morphological investigations.

By means of SFM analysis different morphologies have been observed, namely, flat islands and needle-like objects. Furthermore, it was found that the area covered by islands is declining with increasing substrate temperature, whereas the sample area covered by needles is constant over the investigated temperature range (60–135 °C). Consequently we can draw the conclusion that needle-like structures are energetically more stable as compared to flat islands formed of standing 6T molecules on KCl (100). Additionally, different activation energies for the growth of nanoneedles in height and width have been deduced from SFM analysis, namely, 0.26 ± 0.02 eV and 0.15 ± 0.04 eV, respectively.

By means of XRD specular scans it was possible to determine the contact planes of the structures on the surface. Needles with {010} and {411} and islands with the {100} facet parallel to the substrate surface have been detected. Utilizing XRD pole figures and FFT analysis of optical microscope images we observed that there is a well-defined azimuthal alignment of the structures on the surface in addition to the stacking in growth direction. Notably structures with {100} and {411} contact planes are in perfect azimuthal alignment to each other, which is explained by ledge directed epitaxy of the islands on the sidewalls of already existing needles.

The orientation of the crystallographic structures which are present on the substrate surface fulfills the growth model for rodlike molecules on sheet silicate substrates developed by Simbrunner et al.²⁰ Therein it is explained that the adsorption

of a single molecule dominates in a first step and the nucleation of organic crystallites which follows thereafter only leads to a slight reorientation of the LMAs. Nevertheless substrate surface symmetry plays a major role. In particular rotational and mirror symmetries have to be reflected by the formed needle orientations. The latter considerations are substantiated by the results presented in this paper. The 4-fold rotational symmetry and the mirror symmetry of the KCl (100) substrate surface leads to eight distinct growth directions of each crystal type. Moreover two different crystal contact planes, namely, {010} and {411}, are characterized by an analogous LMA orientation as similarly observed for *p*-hexaphenyl on KCl (100).³⁰ This hints that the adsorption geometry of single molecules seems to be decisive for the organic crystal nucleation as expected by the growth model. The fact that one adsorption geometry can lead to different crystal contact planes may be explained by polymorphs of the first monolayer, that are both based on the same azimuthal orientation of the LMA on the substrate surface. The argument is supported by the fact that monolayer polymorphs of 6T have already been reported on Ag (001)³⁷ and Ag (110).³⁸

Concluding the latter discussion it can be stated that the azimuthal alignment of the organic crystals and molecules is basically determined by a two step process. The initial phase is dominated by the adsorption of single molecules in their energetically preferred adsorption geometry on the substrate surface. This adsorption process is mainly determined by an interplay between substrate geometry, molecular geometry and importantly symmetry properties. In the second step, where the organic crystal nucleation takes place, only a slight azimuthal realignment of the molecules can be caused in order to optimize the lattice match at the interface.

■ ASSOCIATED CONTENT

§ Supporting Information

A complete set of SFM images of 6T deposited on KCl, additional X-ray pole figure measurements and optical microscope images along with their Fourier transformations. This material is available free of charge via the Internet at <http://pubs.acs.org>.

■ AUTHOR INFORMATION

Corresponding Author

*E-mail: guenther.schwabegger@jku.at

Notes

The authors declare no competing financial interest.

■ ACKNOWLEDGMENTS

This work has been financially supported by the Austrian Science Fund (FWF): project numbers NFN-S9706, NFN-S9708, 25154-N20 and by the federal government of Upper Austria (project “Organische Nanostrukturen”).

■ REFERENCES

- (1) Reineke, S.; Lindner, F.; Schwartz, G.; Seidler, N.; Walzer, K.; Lussem, B.; Leo, K. *Nature* **2009**, *459*, 234–238.
- (2) Simbrunner, C.; Hernandez-Sosa, G.; Baumgartner, E.; Hesser, G.; Roither, J.; Heiss, W.; Sitter, H. *Appl. Phys. Lett.* **2009**, *94*, 073505.
- (3) Griesser, T.; Radl, S. V.; Koepllmayr, T.; Wolfberger, A.; Edler, M.; Pavitschitz, A.; Kratzer, M.; Teichert, C.; Rath, T.; Trimmel, G.; Schwabegger, G.; Simbrunner, C.; Sitter, H.; Kern, W. *J. Mater. Chem.* **2012**, *22*, 2922–2928.

- (4) Briseno, A. L.; Mannsfeld, S. C. B.; Reese, C.; Hancock, J. M.; Xiong, Y.; Jenekhe, S. A.; Bao, Z.; Xia, Y. *Nano Lett.* **2007**, *7*, 2847–2853.
- (5) Facchetti, A. *Mater. Today* **2007**, *10*, 28–37.
- (6) Schwabegger, G.; Ullah, M.; Irimia-Vladu, M.; Baumgartner, M.; Kanbur, Y.; Ahmed, R.; Stadler, P.; Bauer, S.; Sariciftci, N.; Sitter, H. *Synth. Met.* **2011**, *161*, 2058–2062.
- (7) Law, M.; Greene, L. E.; Johnson, J. C.; Saykally, R.; Yang, P. *Nat. Mater.* **2005**, *4*, 455–459.
- (8) Dennler, G.; Scharber, M. C.; Brabec, C. J. *Adv. Mater.* **2009**, *21*, 1323–1338.
- (9) Tsiminis, G.; Wang, Y.; Shaw, P. E.; Kanibolotsky, A. L.; Perepichka, I. F.; Dawson, M. D.; Skabara, P. J.; Turnbull, G. A.; Samuel, I. D. W. *Appl. Phys. Lett.* **2009**, *94*, 243304.
- (10) Zhao, Y. S.; Fu, H.; Peng, A.; Ma, Y.; Liao, Q.; Yao, J. *Acc. Chem. Res.* **2010**, *43*, 409–418.
- (11) Quochi, F. *J. Opt.* **2010**, *12*, 024003.
- (12) Simbrunner, C.; Quochi, F.; Hernandez-Sosa, G.; Oehzelt, M.; Resel, R.; Hesser, G.; Arndt, M.; Saba, M.; Mura, A.; Bongiovanni, G.; Sitter, H. *ACS Nano* **2010**, *4*, 6244–6250.
- (13) Simbrunner, C.; et al. *ACS Nano* **2012**, *6*, 4629–4638.
- (14) Horowitz, G.; Garnier, F.; Yassar, A.; Hajlaoui, R.; Kouki, F. *Adv. Mater.* **1996**, *8*, 52–54.
- (15) Liu, S.; Mannsfeld, S. C. B.; Wang, W. M.; Sun, Y.-S.; Stoltzenberg, R. M.; Bao, Z. *Chem. Mater.* **2009**, *21*, 15–17.
- (16) Koini, M.; Haber, T.; Berkebile, S.; Koller, G.; Ramsey, M.; Resel, R.; Oehzelt, M. *J. Cryst. Growth* **2009**, *311*, 1364–1369.
- (17) Simbrunner, C.; Hernandez-Sosa, G.; Oehzelt, M.; Djuric, T.; Salzmann, I.; Brinkmann, M.; Schwabegger, G.; Watzinger, I.; Sitter, H.; Resel, R. *Phys. Rev. B* **2011**, *83*, 115443.
- (18) Albonetti, C.; Barbalinardo, M.; Milita, S.; Cavallini, M.; Liscio, F.; Moulin, J.-F.; Biscarini, F. *Int. J. Mol. Sci.* **2011**, *12*, 5719–5735.
- (19) Walker, D.; Verma, P. K.; Cranswick, M. D.; Jones, R. L.; Clark, S. M.; Buhre, S. *Am. Mineral.* **2004**, *89*, 204–210.
- (20) Simbrunner, C.; Nabok, D.; Hernandez-Sosa, G.; Oehzelt, M.; Djuric, T.; Resel, R.; Romaner, L.; Puschnig, P.; Ambrosch-Draxl, C.; Salzmann, I.; Schwabegger, G.; Watzinger, I.; Sitter, H. *J. Am. Chem. Soc.* **2011**, *133*, 3056–3062.
- (21) Sitter, H.; Andreev, A.; Matt, G.; Sariciftci, N. S. *Mol. Cryst. Liq. Cryst.* **2002**, *385*, 51–60.
- (22) Schulz, L. G. *J. Appl. Phys.* **1949**, *20*, 1030–1033.
- (23) Kankate, L.; Balzer, F.; Niehus, H.; Rubahn, H.-G. *Thin Solid Films* **2009**, *518*, 130–137.
- (24) Biscarini, F.; Zamboni, R.; Samor, P.; Ostoja, P.; Taliani, C. *Phys. Rev. B* **1995**, *52*, 14868–14877.
- (25) Kankate, L.; Balzer, F.; Niehus, H.; Rubahn, H.-G. *J. Chem. Phys.* **2008**, *128*, 084709.
- (26) Horowitz, G.; Bachet, B.; Yassar, A.; Lang, P.; Demanze, F.; Fave, J.-L.; Garnier, F. *Chem. Mater.* **1995**, *7*, 1337–1341.
- (27) Leclerc, P.; Surin, M.; Viville, P.; Lazzaroni, R.; Kilbinger, A. F. M.; Henze, O.; Feast, W. J.; Cavallini, M.; Biscarini, F.; Schenning, A. P. H. J.; Meijer, E. W. *Chem. Mater.* **2004**, *16*, 4452–4466.
- (28) Loi, M. A.; da Como, E.; Dinelli, F.; Murgia, M.; Zamboni, R.; Biscarini, F.; Muccini, M. *Nat. Mater.* **2005**, *4*, 81–85.
- (29) Haber, T.; Ivancic, J.; Ramsey, M.; Resel, R. *J. Cryst. Growth* **2008**, *310*, 101–109.
- (30) Haber, T.; Andreev, A.; Thierry, A.; Sitter, H.; Oehzelt, M.; Resel, R. *J. Cryst. Growth* **2005**, *284*, 209–220.
- (31) Carter, P. W.; Ward, M. D. *J. Am. Chem. Soc.* **1993**, *115*, 11521–11535.
- (32) Bonafede, S. J.; Ward, M. D. *J. Am. Chem. Soc.* **1995**, *117*, 7853–7861.
- (33) Kintzel, J., E. J.; Smilgies, D.-M.; Skofronick, J. G.; Safron, S. A.; Winkle, D. H. V. *J. Vac. Sci. Technol., A* **2004**, *22*, 107–110.
- (34) Frank, P.; Winkler, A. *Appl. Phys. A: Mater. Sci. Process.* **2008**, *90*, 717–721.
- (35) Haber, T.; Resel, R.; Andreev, A.; Oehzelt, M.; Smilgies, D.-M.; Sitter, H. *J. Cryst. Growth* **2010**, *312*, 333–339.
- (36) Mikami, T.; Yanagi, H. *Appl. Phys. Lett.* **1998**, *73*, 563–565.
- (37) Duncker, K.; Kiel, M.; Höfer, A.; Widdra, W. *Phys. Rev. B* **2008**, *77*, 155423.
- (38) Wagner, T.; Fritz, D. R.; Zeppenfeld, P. *Synth. Met.* **2011**, *161*, 2006–2010.